Open access • Journal Article • DOI:10.1007/S11548-019-02080-3

Body-mounted robotic assistant for MRI-guided low back pain injection

Gang Li, Niravkumar Patel, Jan Hagemeister, Jiawen Yan ...+4 more authors

Institutions: Johns Hopkins University

Published on: 01 Feb 2020 - International Journal of Computer Assisted Radiology and Surgery (Int J Comput Assist Radiol Surg)

Topics: Imaging phantom and Image quality

Remotely Actuated Needle Driving Device for MRI-Guided Percutaneous Interventions

Di Wu*†,Gang Li*, Niravkumar Patel*, Jiawen Yan*, Reza Monfaredi‡, Kevin Cleary‡ and Iulian Iordachita*
*Laboratory for Computational Sensing and Robotics,
Johns Hopkins University, Baltimore, MD 21218, USA
†Department of Mechanical Engineering,
Technical University of Munich, Garching 85748, Germany
‡Childrens National Medical Center,
111 Michigan Avenue, NW Washington, DC 20010
Email: dwu39@jhu.edu

***Abstract*—In this paper we introduce a remotely actuated MRI-compatible needle driving device for pain injections in the lower back. This device is able to manipulate the needle inside the closed-bore MRI scanner under the control of the interventional radiologist inside both the scanner room and the console room. The device consists of a 2 degrees of freedom (DOF) needle driver and an actuation box. The 2-DOF needle driver is placed inside the scanner bore and driven by the actuation box settled at the end of the table through a beaded chain transmission. This novel remote actuation design could reduce the weight and profile of the needle driver that is mounted on the patient, as well as minimize the potential imaging noise introduced by the actuation electronics. The actuation box is designed to perform needle intervention in both manual and motorized fashion by utilizing a mode switch mechanism. A mechanical hard stop is also incorporated to improve the device's safety. The bench-top accuracy evaluation of the device demonstrated a small mean needle placement error (< 1 mm) in a phantom study.**

***Index Terms*—pain management, needle driving device, beaded chain transmission, remote actuation, MRI-guided intervention.**

I. INTRODUCTION

Chronic pain management is a significant clinical challenge in both adult and pediatric patients, and the global pain management devices market is expected to reach USD 8.6 billion by 2022 [1]. Needle-based interventional pain management is one approach to cope with pain in the treatment cycle. In the diagnosis of patients with chronic neuropathic pain, perineural injection of topical anesthetics is widely used. Once the diagnosis is made, injection of steroids is an effective way to achieve long-lasting pain relief [2]. Sometimes, medications including phenol and ethanol that cause denervation are injected to destroy the source of the pain [3]. These injection procedures are normally carried out under CT, ultrasound or fluoroscopy guidance.

We aim to enable MRI-guided lower back pain injections, as MRI provides high contrast soft tissue imaging without ionizing radiation. In MRI-guided interventions, the bevel-tip needles is a commonly-used tool because of its steerability and flexibility, and thus it is able to be steered away from obstacles (e.g. hard tissue, bone, nerve, etc.) to reach the target [4]. However, it could be very hard to steer the needle manually without the intraoperative continuous image feedback. Therefore, MRI-guided interventions can be a challenging and multi-step process due to repeating imaging and verification. These procedures could be time-consuming, especially moving the patient iteratively in and out of the scanner bore resulting in possible anxiety for the patient. In addition, such multi-step MRI-guided procedures may lead to other problems like longer occupation of the MRI scanner, more treatment expense and more workload of the interventional radiologist.

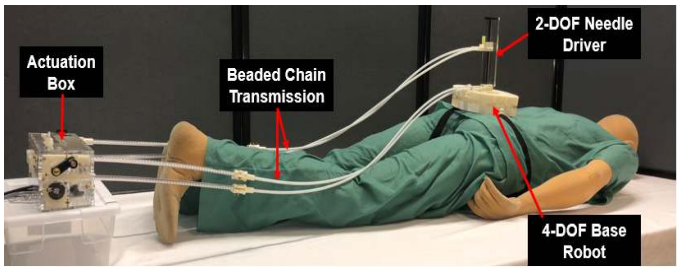

Fig. 1. The new robotic system that assists needle steering during MRI-guided intervention for pain management. The 2-DOF needle driver is attached onto the current version of our 4-DOF base robot, and aims toward a 6-DOF robotic platform. The needle driver is remotely actuated by the actuation box through beaded chain transmission.

Robotic assistance provides an approach with greater precision and enhanced dexterity for needle steering. However, it still suffers from a few challenges in the MRI environment due to the narrow space and high-intensity magnetic field in the MRI scanner bore [5]. These conditions impose a few restrictions on the device design. A few researches have reported on the MRI-compatible needle driver or robotic needle guidance for various application including prostate biopsy [6], [7], liver interventions [8], pelvis interventions [9], breast intervention [10] and neurosurgery [11]. Furthermore, to allow the clinician to remotely steer the needle outside the scanner bore, alleviate the need to move the patients in and out of the scanner, and streamline the workflow, several research groups have worked on the remote actuation of needle

This work was funded by National Institutes of Health under grant number 1R01 EB025179-01.

978-1-5386-7825-1/19/$31.00 ©2019 IEEE

placement. The possibility of actuating MRI-compatible haptic interfaces through a long cable transmission was studied in [12]. A similar use of cable transmission was presented in the Neuroblate® robotic probe for laser ablation [13], [14], and the clinical trials and technical details were reported in [15], [16]. Hydraulic and pneumatic transmissions have also been studied to implement remote actuation. Burkhard et al. [17] developed a 1-DOF novel bilateral teleoperator for needle insertion using both pneumatic and hydraulic transmissions. A hydraulic driving robot [18] was designed by Guo et al. for intraoperative MRI-guided bilateral stereotactic neurosurgery. A master-slave configuration is a solution for teleoperation as well. Seifabadi et al. designed a 2-DOF master robot to remotely actuate a 2-DOF needle steering module connected by a pneumatic transmission [19].

Previously, our group has developed a body-mounted serial robot [20] for aligning the needle entry point, and a series of experiments were completed to verify its accuracy [21], [22]. To increase the rigidity of the robot and optimize the mass distribution, a parallel robot [23] was subsequently proposed.

This work introduces a remotely actuated needle driving device (shown in Fig.1) that can be mounted on the previously designed serial or parallel base robot [22], [23]. It is designed to accurately steer and place the needle for injections around nerves to treat pain in adult and pediatric patients under real-time MRI-guidance while keeping the clinician in control. The main contributions of this paper are: 1) Design a novel remotely actuated needle driving device, which could reduce patient-end device weight and size, alleviate imaging noise, enhance ergonomic, and optimize the clinical workflow. This is, to the best of our knowledge, the first time that the beaded chain transmission is used in an MRI-guided robotic system. 2) Develop a mode switch mechanism that enables intervention in both manual and motorized fashion. For the sake of safety, manual needle invention could be performed alternatively in case of motorization failure. 3) Design a mechanical hard stop that provides a safety factor if the encoders fail. 4) Evaluate the system accuracy in both free space and phantom studies. 5) Validate the functionality of the device in the MRI environment.

II. Needle Driving Device System Design

TABLE I
THE DESIGN REQUIREMENTS BASED ON CLINICAL STUDIES

Requirements	Value
Insertion Accuracy	<0.5 mm
Rotation Accuracy	<5 deg
Insertion Backlash	<0.5 mm
Rotation Backlash	<1 deg
Overall Length	<200 mm
Insertion Depth	50-150 mm
Overall Weight	<200 g
Targeting Accuracy in Phantom	<1 mm

Based on the clinical studies [24], [25] of needle-based percutaneous interventions, the design requirements are derived as listed in Table I. This device as shown in Fig. 2 consists of the needle driver, the beaded chain transmission, and the actuation box, which enables the clinicians to remotely manipulate the needle inside the scanner bore under the real-time MRI-guidance.

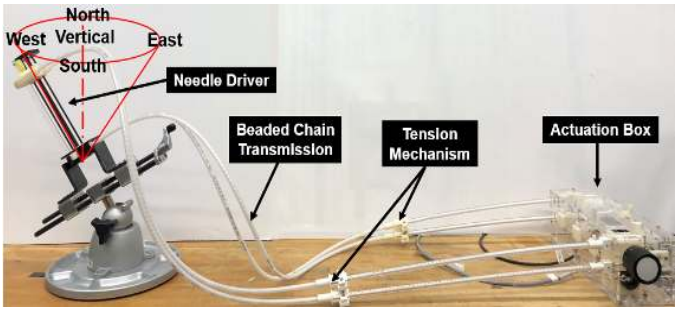

Fig. 2. Main components of the needle driving device. The actuation box can remotely actuate the needle driver through a 1.2 meters long beaded chain transmission.

A. Needle Driver

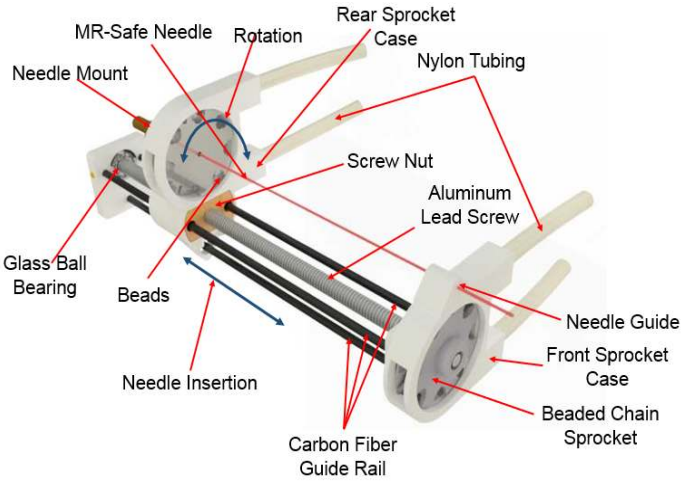

Fig. 3. The CAD model demonstrating the components of the needle driver and its translation and rotation motion.

The needle driver, which is remotely driven by the beaded chain, is a 2-DOF end-effector of the system. It is capable of steering the needle inside the scanner bore. Its structure and degrees of freedom are shown in Fig. 3. The needle manipulation consists of needle insertion and rotation. The needle insertion employs the lead screw mechanism to convert the rotation motion of the sprocket into translation. Three carbon fiber rods work as the guide rail to increase the device rigidity and ensure straight translation. Considering the requirements of deep insertion in lower back, the overall length of the needle driver is 186 mm with an effective insertion depth of 150 mm, its overall size allows it to fit in a standard scanner bore (Fig. 7(a)). The diameter and pitch of the screw are 6.35 mm and 5.08 mm respectively. The rotation is directly actuated by the beaded chain, and it is capable of achieving 360° rotation. The mounting adapter is placed on the rotation

sprocket, where an MRI-safe disposable needle can be easily mounted via a locking mechanism. A 10-mm-long needle guide is integrated with the front sprocket case to hold the needle.

To ensure MRI-compatibility, the needle driver is made of 3D printed Acrylonitrile butadiene styrene (ABS), ceramic ball bearings, aluminum lead screw, and laser cut acrylic plate. Since these are all light-weight materials, the overall weight of the needle driver is minimal at 120 grams. Furthermore, there are no electronic elements on the needle driver, thus artifacts on the MR imaging could be alleviated.

B. Beaded Chain Transmission

The actuation box is placed at the end of the MRI table to avoid introducing artifacts. Accordingly the main requirements for the transmission are: 1) It should be long enough. Considering the average height of adult men and various insertion locations, the transmission length should be between 0.8 m to 1.2 m. 2) It should be a flexible transmission, because the needle driver may have various orientations with respect to the actuation box. Based on these requirements, we adopted a beaded chain transmission. The diameter of the plastic beaded chain (BlindsOhMy Co., China) is 4.5 mm and the chain pitch is 6mm. Of note, there is neither commercially available beaded chain sprocket (as standalone product) nor ready-made theory for sprocket design. Hence, the build-verify-test strategy was used to continuously optimize the size and profile of the sprocket (shown in Fig. 4(a)). The outer diameter of the latest generation of sprocket is 34 mm with 15 teeth on it. As shown in Fig. 4(c), the profile of the teeth is different in the opposite direction: one edge is triangular, the other one is arc and they are staggered. This design contributes to the alignment of the beaded chain and provides smooth engagement and disengagement between the chain and sprocket. A plastic tubing (Freelin-Wade Co., OR, USA), OD=6.35 mm, ID=4.57 mm, made of super soft nylon was employed to provide the tension and work as a guiding sleeve for the beaded chain. The procedures for connecting the beaded chain are as follows: 1) Loosen the tensioning mechanism. 2) Thread the beaded chain through the tubing and sprockets. 3) Melt the two half beads by a soldering iron(beads are made of thermoplastic material). 4) Merge two half beads into one by pressing. 5) Tension the beaded chain with tensioning mechanism.

C. Actuation Box

The actuation box (Fig. 5) consists of an upper box and a lower box that are made of acrylic plates. The lower box contains the piezo motors (LR 50, PiezoMotor Co., Upsala, Sweden), encoders (US Digital, WA, USA) and cables. For both translation and rotation, the power is transmitted from the lower box to the upper box by a pair of spur gears (gear ratio 1:1). The sprockets are mounted coaxially with the gears thereby the beaded chain can be driven to insert or rotate the needle. In terms of translation, there is a 2-branch transmission after the spur gears. In the opposite direction of

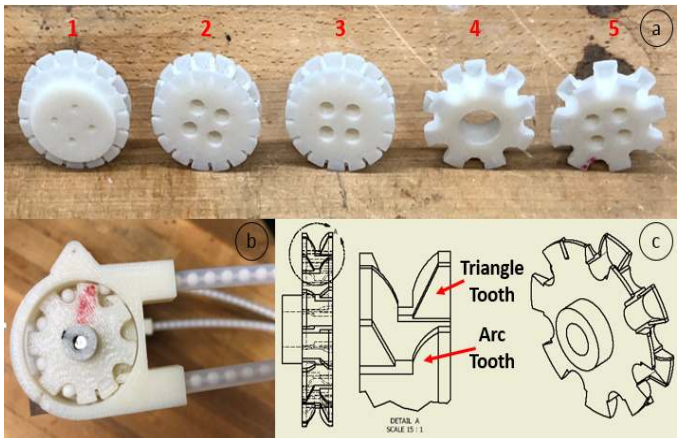

Fig. 4. Sprocket design: (a) Iterative design of the sprockets. The rightmost prototype is currently used in the device. (b) Assembly of sprocket, beaded chain and nylon tubing. (c) Asymmetrical teeth smoothing the engagement between the chain and sprocket.

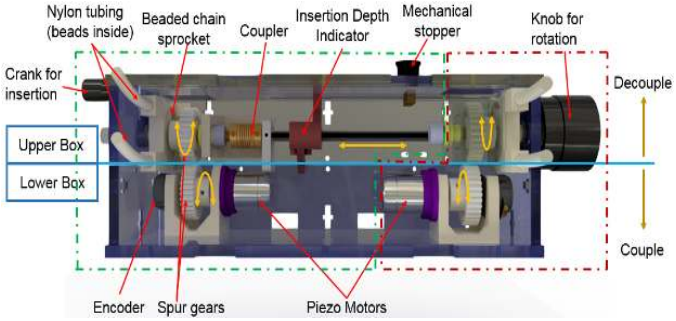

Fig. 5. CAD model of the actuation box showing its components and internal motions. The presented setup is the motorized mode, the gears are engaged. Once the upper box is lifted up, the gears will be separated and will switch to manual mode.

the sprocket, a lead screw mechanism is connected through a coupler (S50HAWM15H0404, SDP/SI, NY, USA) to translate the insertion depth indicator.

To improve the needle insertion safety, the actuation box is equipped with a mechanical hard stop and a second lead screw transmission that has the same size as the one on the needle driver. Being mechanically coupled, both lead screw transmissions are moving in the same time with the same travel and hence the insertion depth indicator (Fig. 5) and the screw nut (Fig. 3) are moving synchronously. The mechanical hard stop can be fixed to a desired insertion depth by the operator by adjusting the wing nut. Once the insertion depth indicator reaches the stopper, the transmission system will automatically stop the screw nut at the desired insertion depth.

A mode switch function between the motorized insertion and manual insertion is designed to provide two choices for the operation and a backup plan if the motors fail. There are 5 sliders with dovetail slot and matching guided rails on the outer surface of the upper and lower box respectively so they can be moved to be coupled or decoupled. If the upper box is lifted up, the two boxes are decoupled and the clinician can

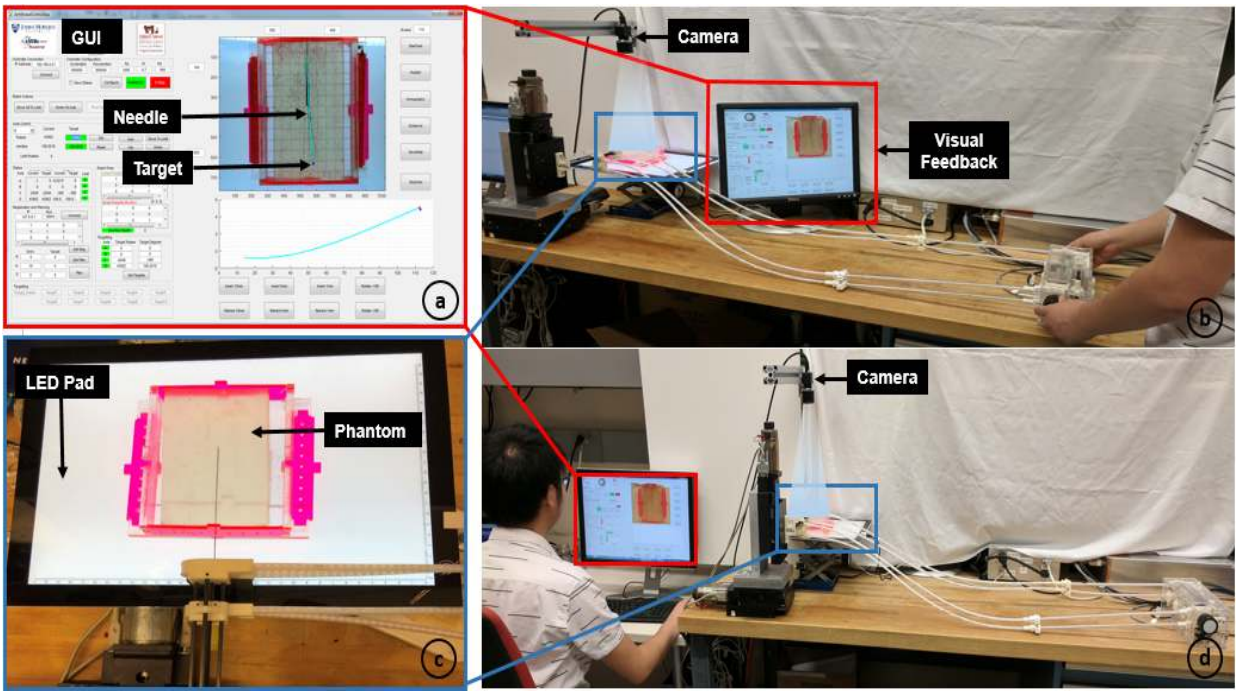

Fig. 6. Bench-top experimental setup: (a) The Matlab based GUI showing the position of needle tip and target and reconstructed the needle shape. (b) User run the manual insertion by rotating the crank and the knob with camera image feedback via control GUI. (c) Artificial phantom simulating the soft tissue and the LED pad lightening the phantom. (d) User run the motorized insertion by clicking the insertion and rotation buttons on the GUI.

carry out the manual insertion by using the hand crank and knob on the side of the box (Fig. 5).

D. Control System and User Interface

The control system is developed based on an industrial grade 4-axis controller (Galil Motion Control, Rocklin, CA, USA) to provide real-time closed-loop control of the piezomotors [22]. The controller provides interfaces for 4 differential encoders, 1 limit switch per axis, emergency stop switch and user configurable motor driver interface. The motor driver interface was configured to control the Piezo LEGS motor, while the differential encoders from US Digital are configured for quadrature encoding for higher resolution. An intuitive Graphical User Interface (GUI) as shown in Fig. 6a was developed based on [22] to help the clinicians when operating the device. They can observe the real-time imaging generated from MRI and take actions by just clicking the buttons on the panel. The GUI panel can be extended to integrate the imaging feedback from the camera for laboratory bench testing.

III. EXPERIMENTS AND RESULTS

A. Accuracy and Repeatability Assessment

This assessment was performed to evaluate the accuracy of the device in free space. The experimental setup is shown in Fig. 2. The needle driver was mounted on a 3-DOF base mount (Model 350, Panavise Inc, USA). The distance between the needle driver and the actuation box was changed between 110 cm and 85 cm, simulating two extreme insertion positions at lower back. At each transmission length, five poses (i.e. vertical, south, north, west and east, Fig. 2) were configured to assess its performance under various orientation. Except for the vertical orientation, all the other poses have a 30° angle with respect to the centerline, which was measured by a digital level (Checkpoint Inc., USA, precision 0.1°). At each configuration, the needle was inserted with three different depths (50 mm, 70 mm, 100 mm) and each insertion was repeated three times after the homing procedure. The insertion depths were measured with a caliper (500-196, Mitutoyo Co., Japan, resolution 0.01 mm).

As for the rotation, an angle gauge was attached to the rear sprocket case (Fig. 3) as a reference to measure the rotation angle. The needle was rotated 180° ten times when the actuation box was placed at 120 mm distance.The accuracy and repeatability results of both translation and rotation are summarized in Table II. A translation error less than 0.35 mm and a rotation error smaller than 2.25° validated the feasibility of the novel beaded chain transmission.

B. Backlash Assessment and Compensation

Backlash was assessed since the needle may be retracted and reversely rotated to amend its trajectory. An experimental setup similar to the one used for accuracy assessment and a dial indicator (Mitutoyo Corp., Japan, resolution 0.001mm) were utilized in this experiment. To evaluate the translation backlash, 2 mm insertions and retractions were subsequently carried out ten times. The translation backlash was defined as the variation of the needle position after 2 isometric movements. Similarly, using the same angle gauge as in the

TABLE II
RESULTS OF THE ACCURACY AND REPEATABILITY ASSESSMENT

Motion	Transmission Length	Orientation	MEAN	STD
Translation (mm)	110 cm	Vertical	-0.166	0.129
		North	-0.220	0.115
		South	-0.149	0.131
		West	-0.252	0.108
		East	-0.337	0.063
		Overall	-0.225	0.131
	85 cm	Vertical	-0.226	0.106
		North	-0.187	0.037
		South	-0.209	0.111
		West	-0.164	0.103
		East	-0.132	0.071
		Overall	-0.182	0.096
Rotation (deg)	120 cm	Vertical	-2.25	0.722

TABLE III
RESULTS OF THE BACKLASH TEST BEFORE AND AFTER THE COMPENSATION

	Motion	MEAN	STD
Before compenstion	Translation (mm)	1.262	0.008
	Rotation (deg)	3.90	0.943
After compensation	Translation (mm)	0.063	0.060
	Rotation (deg)	0.58	0.640

accuracy assessment, the sprocket was rotated 180° and rolled back to the home position. The variation of the angles were considered as rotation backlash. Both tests were carried out 10 times and the average value and standard deviation are summarized in Table III (Before Compensation). The backlash originated from the beaded chain to sprockets play and lead screw to nut play.

To compensate the backlash, a software compensation method was implemented in the control system. The control system detected the motion direction based on the position feedback. Once the direction of the motion was changed, the control system set a new target with a compensating offset based on mean backlash errors measured in the experiment. The backlash assessment experiment was repeated with the software compensation, and the results were summarized in Table III (After Compensation). The results indicated that the compensation method could effectively compensate the mechanical backlash.

C. Bench-top Needle Steering Accuracy Evaluation

The system accuracy was further evaluated in phantom studies under camera image feedback. The experimental setup is shown in Fig. 6. The needle driver was mounted on a 3-DOF linear stage. The artificial phantom was made of liquid plastic and plastic hardener (M-F Manufacturing Company, TX, US) with a ratio of 5:2. A camera (FL2-08S2C, FLIR Integrated Imaging Solutions Inc., OR, USA) for capturing the needle trajectory was mounted above the phantom at an appropriate height and the captured images were sent back to the GUI as visual feedback for users. The pixel size of the camera image is 0.2mm x 0.2mm. The user first chooses a target on the GUI and the target remains fixed during the entire insertion procedure. Under the real-time camera image feedback, the user steers it to the target by predicting the critical turning point and reorienting the bevel according to the needle trajectory. After the insertion procedure is finished, the user evaluates the targeting error. In this experiment the error is defined as the distance between needle tip and target position, both displayed on the GUI (Fig.6). Ten manual insertions and ten motorized insertions were carried out. The errors and standard deviation are presented in Table IV and Table V. By analyzing the results, both the errors of manual and motorized insertions are around 0.8 mm.

TABLE IV
RESULTS OF THE NEEDLE STEERING EXPERIMENT SHOWING THE ERRORS BY MANUAL INSERTION (UNITS ARE IN MM)

No.	Target		Actual Tip		Errors		
	x	y	x	y	x	y	mag
1	109.89	4.65	109.92	4.61	0.03	-0.04	0.05
2	110.26	-4.91	110.03	-5.73	-0.23	-0.83	0.86
3	109.96	-6.95	109.68	-7.28	-0.28	-0.33	0.44
4	109.81	2.15	110.36	1.77	0.55	-0.38	0.67
5	99.94	-4.94	100.68	-6.10	0.74	-1.16	1.38
6	99.95	1.80	100.41	1.06	0.46	-0.75	0.87
7	105.16	-6.67	105.27	-7.75	0.11	-1.08	1.09
8	109.83	1.88	109.86	0.96	0.03	-0.92	0.92
9	114.39	-7.79	114.80	-8.35	0.41	-0.56	0.70
10	116.46	3.09	116.27	3.69	-0.19	0.60	0.63
Overall				MEAN	0.16	-0.54	0.76
				STD	0.34	0.51	0.34

TABLE V
RESULTS OF THE NEEDLE STEERING EXPERIMENT SHOWING THE ERRORS BY MOTORIZED INSERTION (UNITS ARE IN MM)

No.	Target		Actual Tip		Errors		
	x	y	x	y	x	y	mag
1	112.28	-7.77	112.02	-8.66	-0.26	-0.88	0.92
2	101.67	1.75	101.11	1.46	-0.56	-0.28	0.63
3	111.74	4.13	111.07	3.73	-0.67	-0.39	0.78
4	113.51	-8.01	112.99	-8.24	-0.52	-0.22	0.57
5	112.73	4.87	112.33	3.76	-0.40	-1.12	1.19
6	112.53	-7.40	112.03	-7.89	-0.50	-0.49	0.70
7	112.61	2.87	112.23	1.55	-0.38	-1.32	1.37
8	108.30	-6.20	107.63	-7.05	-0.67	-0.85	1.08
9	114.41	2.85	114.62	3.35	0.21	0.50	0.54
10	115.32	-8.82	115.02	-8.65	-0.30	0.17	0.35
Overall				MEAN	-0.41	-0.49	0.81
				STD	0.24	0.54	0.31

D. Functionality validation in the MRI environment

The device functionality in MRI environment was tested in a scanner (Siemens Aera, 1.5 Tesla) at the Children's National Medical Center, Washington, DC. The same phantom used in the needle steering experiment was employed. Three manual insertions were performed in this test. As shown in Fig. 7, the real-time MR images (flip angle :45°, TR: 228.5ms, TE: 1.4ms, slice thickness: 8mm, pixel spacing: 1.9mm x 1.9mm) were projected onto a screen. The user, by observing the screen and standing next to the scanner table, was able to remotely steer the needle. A high resolution confirmation imaging (flip angle: 150°, TR: 410ms, TE: 14ms, slice thickness: 3.5mm, pixel spacing: 0.39mm x 0.39mm) was taken for each

TABLE VI
NEEDLE TIP ACCURACY IN THE MRI ENVIRONMENT (UNITS ARE IN MM)

Number	Insetion Time	Target			Actual Tip			Error			
		R	A	S	R	A	S	R	A	S	mag
1	2’	-6.83	-3.42	7.45	-7.00	-3.40	11.40	-0.17	0.02	3.95	3.95
2	1’55”	-6.83	-11.45	17.47	-7.00	-11.50	19.00	-0.17	-0.05	1.53	1.54
3	1’50”	-7.61	-13.25	12.55	-7.40	-13.20	14.40	0.21	0.05	1.85	1.86
Overall							MEAN	-0.04	0.01	2.44	2.45
							STD	0.18	0.04	1.07	1.07

target to analyze the needle steering accuracy. The errors and insertion time are recorded in Table VI. The first insertion was performed using only the body coils for imaging. The image artifact around the needle was relatively large, which led to a relatively large insertion error. By placing 2 flexible imaging coils around the needle driver, the image artifact was reduced, and the insertion accuracy was increased.

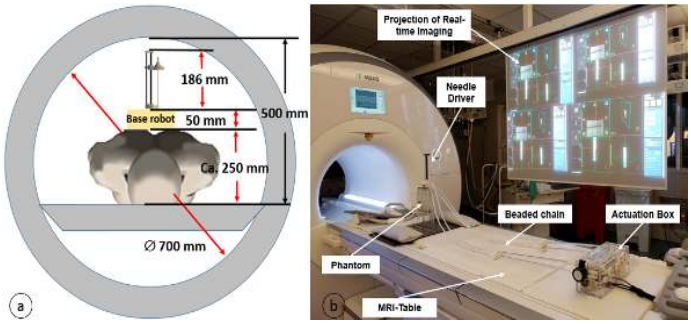

Fig. 7. System was tested in MRI room: (a) Parameterized schematic showing the patient and robotic system inside a standard 70 cm aperture MRI scanner. (b) Experimental setup in the MRI room. Needle driver is placed inside the scanner bore, and the actuation box is placed at the end of the table. The user could manually steer the needle while observing the real-time MR images projected on the screen.

IV. DISCUSSION

The results of the accuracy and repeatability tests reveal a mean error of -0.225 mm and -0.182 mm at the transmission length of 110 cm and 85 cm respectively, while the mean rotation error is -2.25°. All the results satisfy the requirements in Table I. The small standard deviations reveal good repeatability of the transmission. Moreover, the similar performance at different transmission lengths and orientations demonstrate its consistency and stability with varied configurations.

The backlash of the device was 1.262 mm in translation and 3.9° in rotation, which are the inherent errors of the system accumulating from multiple sources such as the play between the spur gears, beads and sprocket along with the screw nut and lead screw. After the software compensation, the backlashes were significantly reduced to 0.063 mm and 0.58° respectively, which is sufficient for retracting or reversely rotating the needle.

The needle steering accuracy evaluation with camera image feedback shows that there is a similar accuracy between the manual insertion (0.76 mm) and motorized insertion (0.81 mm). The small standard deviation in both cases reveal a high repeatability of steering the needle.

In the MRI test, all the insertions were performed within 2 minutes. The accuracy of the last 2 insertions were remarkably improved ($<$ 2 mm) after we placed the flexible imaging coils, but the mean error in the MRI environment (2.45mm) is still bigger than the bench-top experiments and also over the requirement (2 mm) in Table I. Due to the artifact of the needle, its appearance in the images is larger than its actual dimensions, which influence the users’ ability to place the needle, hence the errors were increased.

In the future we plan to run more experiments in the MRI environment and to optimize the imaging sequences to reduce the artifacts. Moreover, we will begin to develop a new generation of the needle driving device with improved performances. In addition, motorized insertion experiments will be carried out in the MRI to systematically evaluate the device functionality.

V. CONCLUSION

In this paper a remotely actuated needle driving device for MRI-guided interventions in pain management was developed and validated. It is able to extend the controllable range of a clinician into the scanner bore while keeping the clinician in the loop, which may simplify the clinical procedure, improve the precision and enhance the safety. The innovative features are the beaded chain transmission, the mode switch between manual and motorized, and mechanical hard stop.

The accuracy, repeatability, and backlash of both the device translation and rotation were experimentally measured and the backlash was further compensated through software. The needle steering accuracy evaluation with camera image feedback demonstrated the feasibility of this proof-of-concept device, and both manual and motorized insertions were carried out ten times into a phantom. The results revealed that the device can provide needle tip placement with less than 0.8 mm mean error in lab studies. This is an ongoing project, and the future work includes the device structure optimization and its integration with the base robot.

VI. ACKNOWLEDGE

We would like to acknowledge the assistance of our Children’s colleagues Lu Vargas and Eleni Siampli in conducting the MRI experiments.

REFERENCES

[1] Grand View Research, Pain Management Devices Market Worth $8.6 Billion By 2022. [Online]. Available: https://www.grandviewresearch.com/press-release/global-pain-management-devices-market. [Accessed: 23-Dec-2016].

[2] J. Lee, S. Choi, E. Ahn, K. Hahm, J. Suh, J. Leem et. al., "Effect of perioperative perineural injection of dexamethasone and bupivacaine on a rat spared nerve injury model," The Korean journal of pain 2010 vol: 23 (3) pp: 166-71

[3] D. Koyyalagunta, M. Engle, J. Yu, L. Feng, D. Novy, "Retrospective Evaluation The Effectiveness of Alcohol Versus Phenol Based Splanchnic Nerve Neurolysis for the Treatment of Intra-Abdominal Cancer Pain. " Pain Physician 2016 vol: 19 pp: 281-292

[4] R. Alterovitz, K. Goldberg, and A. Okamura, Planning for Steerable Bevel-tip Needle Insertion Through 2D Soft Tissue with Obstacles. In:Proceedings of the 2005 IEEE International Conference on Robotics and Automation. 2005, pp. 1640-1645.

[5] R. Gassert, E. Burdet, and K. Chinzei, Opportunities and challenges in MR-compatible robotics, IEEE Eng. Med. Biol. Mag., vol. 27, no. 3, pp. 15-22, 2008.

[6] M. Li, G. Li, B. Gonenc, X. Duan, and I. Iordachita, Towards human-controlled, real-time shape sensing based flexible needle steering for MRI-guided percutaneous therapies. In:The International Journal of Medical Robotics and Computer Assisted Surgery 2017 vol: 13 (2) pp: e1762.

[7] N.A. Patel, G. Li, W. Shang, M. Wartenberg, T. Heffter, E.C. Burdette, I. Iordachita et. al., 2018. System Integration and Preliminary Clinical Evaluation of a Robotic System for MRI-Guided Transperineal Prostate Biopsy. Journal of Medical Robotics Research, 2018 pp: 1950001

[8] S. E. Song, J. Tokuda, K. Tuncali, A. Yamada, M. Torabi, and N. Hata, Design evaluation of a double ring RCM mechanism for robotic needle guidance in MRI-guided liver interventions. In:IEEE International Conference on Intelligent Robotsand Systems, Nov. 2013, pp. 4078-4083.

[9] S. Elayaperumal, M. R. Cutkosky, P. Renaud, and B. L. Daniel, A Passive Parallel Master-Slave Mechanism for Magnetic Resonance Imaging-Guided Interventions. In:Journal of Medical Devices, Mar. 2015, pp. 0110081-1100811.

[10] V. Mallapragada, N.Sarkar, T.Podder, "Toward a Robot-Assisted Breast Intervention System". IEEE/ASME Transactions on Mechatronics, 2011 vol: 16 (6) pp: 1011-1020

[11] G. Li, H. Su, G.A. Cole, W. Shang, K. Harrington, A. Camilo, J.G. Pilitsis, G.S. Fischer, "Robotic System for MRI-Guided Stereotactic Neurosurgery". IEEE transactions on biomedical engineering, 2015vol: 62 (4) pp: 1077-88

[12] D. Chapuis, R. Gassert, G. Ganesh, E. Burdet, and H. Bleuler, Investigation ofa Cable Transmission for the Actuation of MR Compatible Haptic Interfaces.In:The First IEEE/RAS-EMBS International Conference on Biomedical Robotics and Biomechatronics (BioRob), 2006, pp. 426-431.

[13] M. J. LaRiviere and R. E. Gross, Stereotactic laser ablation for medically intractable epilepsy: The next generation of minimally invasive epilepsy surgery, Frontiers Surg., vol. 3, no. 64, 2016.

[14] A. M. Mohammadi and J. L. Schroeder, Laser interstitial thermal therapy intreatment of brain tumors the NeuroBlate System. In:Expert Review of MedicalDevices, Mar. 2014, pp. 109-119.

[15] A. E. Sloan, M. S. Ahluwalia, J. Valerio-Pascua, S. Manjila, M. G. Torchia, S. E. Jones,J. L. Sunshine, M. Phillips, M. A. Griswold, M. Clampitt, C. Brewer, J. Jochum,M. V. McGraw, D. Diorio, G. Ditz, and G. H. Barnett, Results of the NeuroBlate System first-in-humans Phase I clinical trial for recurrent glioblastoma. In:Journalof Neurosurgery, June 2013, pp. 1202-1219.

[16] A. H. Hawasli, W. Z. Ray, R. K. Murphy, R. G. Dacey Jr, and E. C. Leuthardt, Magnetic resonance imaging-guided focused laser interstitial thermal therapy for subinsular metastatic adenocarcinoma: Technical case report, Oper. Neurosurg., vol. 70, pp.332-337, 2011

[17] N. Burkhard, S. Frishman, A. Gruebele, J. P. Whitney, R. Goldman, B. Daniel,and M. Cutkosky, A rolling-diaphragm hydrostatic transmission for remoteMR-guided needle insertion. In:IEEE International Conference on Robotics and Automation. 2017, pp. 1148-1153.

[18] Z. Guo, Z. Dong, K.-H. Lee, C. L. Cheung, H.-C. Fu, J. D. Ho, H. He, W.-S. Poon,D. T.-M. Chan, and K.-W. Kwok, Compact Design of a Hydraulic Driving Robotfor Intraoperative MRI-Guided Bilateral Stereotactic Neurosurgery. In:IEEE Robotics and Automation Letters, July 2018, pp. 2515-2522.

[19] R.Seifabadi, F.Aalamifar, I.Iordachita and G.Fichtinger, "Toward teleoperated needle steering under continuous MRI guidance for prostate percutaneous interventions". The International Journal of Medical Robotics and Computer Assisted Surgery 2016 vol: 12 (3) pp: 355-369

[20] R. Monfaredi, R. Seifabadi, I. Iordachita, R. Sze, N. M. Safdar, K. Sharma, S.Fricke, A. Krieger, and K. Cleary, A Prototype Body-Mounted MRI-Compatible Robot for Needle Guidance in Shoulder Arthrography. In:Proceedings of the IEEE/RAS-EMBS International Conference on Biomedical Robotics and Biomechatronics.(Aug. 2014), pp. 40-45.

[21] R. Monfaredi, E. Wilson, R. Sze, K. Sharma, B. Azizi, I. Iordachita, and K. Cleary, Shoulder-Mounted Robot for MRI-guided arthrography: Accuracy and mountingstudy. In:2015 37th Annual International Conference of the IEEE Engineering in Medicine and Biology Society (EMBC). IEEE, Aug. 2015, pp. 3643-3646.

[22] N. A. Patel, E. Azimi, R. Monfaredi, K. Sharma, K. Cleary, and I. Iordachita, Robotic system for MRI-guided shoulder arthrography: Accuracy evaluation. In:2018 International Symposium on Medical Robotics, ISMR 2018. Vol. 2018-Janua. IEEE, Mar. 2018, pp. 1-6.

[23] J. S. Kim, D. Levi, R. Monfaredi, K. Cleary, and I. Iordachita, A new 4-DOF parallel robot for MRI-guided percutaneous interventions: Kinematic analysis.In:2017 39th Annual International Conference of the IEEE Engineering in Medicine and Biology Society (EMBC). Vol. 2017. IEEE, July 2017, pp. 4251-4255.

[24] Y. Koethe, S. Xu, G. Velusamy, B. Wood, A. Venkatesan, "Accuracy and efficacy of percutaneous biopsy and ablation using robotic assistance under computed tomography guidance: a phantom study." European radiology 2014 vol: 24 (3) pp: 723-30

[25] T. Oliveira-Santos, B. Klaeser, T. Weitzel, T. Krause, L. Nolte, M. Peterhans et. al.,"A navigation system for percutaneous needle interventions based on PET/CT images: Design, workflow and error analysis of soft tissue and bone punctures, " Computer Aided Surgery 2011 vol: 16 (5) pp: 203-219